

Effect of disorder and polarization sequences on two-dimensional spectra of light harvesting complexes

Tobias Kramer · Mirta Rodríguez

10. October 2019

Abstract Two-dimensional electronic spectra (2DES) provide unique ways to track the energy transfer dynamics in light-harvesting complexes. The interpretation of the peaks and structures found in experimentally recorded 2DES is often not straightforward, since several processes are imaged simultaneously. The choice of specific pulse polarization sequences helps to disentangle the sometimes convoluted spectra, but brings along other disturbances. We show by detailed theoretical calculations how 2DES of the Fenna-Matthews-Olson complex are affected by rotational and conformational disorder of the chromophores.

Keywords Two-dimensional spectroscopy · Light-harvesting complex · FMO (Fenna-Matthews-Olson complex)

1 Introduction

The investigation of energy transfer in light-harvesting complexes (LHCs) is naturally performed by optical spectroscopy. To study the time scales and intermediate steps associated with the energy transfer from the antenna to the reaction center requires time- and frequency resolving methods (Blankenship 2014). One example are transient absorption spectra which probe the response of the system after an excitation (pump) pulse. Transient absorption spectra can be described as projected two-dimensional electronic spectra (2DES), which in turn rely on a sequence of four pulses to sepa-

rate the excitation and emission frequencies. The theoretical modeling of 2DES within non-perturbative theories of the exciton dynamics requires considerable computational effort due to the possibility of excited state absorption, giving rise to the presence of two excitons in the molecular complex (Mukamel 1995; Cho 2008; Hamm and Zanni 2011). The excitons are coupled to vibrations of the molecules, which induces decoherence and dissipation. The dissipation directs the excitons to lower lying states, where often the reaction center of LHCs is located (Blankenship 2014).

The first-principle calculation of excitonic site-energies and inter-pigment couplings requires a mixed molecular-dynamics quantum-chemistry approach due to the modulations of the excitonic energies by the solvent and the protein scaffolding, see Olbrich et al. (2011); Aghtar et al. (2013). For typical distances of chromophores in LHCs and at physiological temperatures, a commonly used model is the Frenkel-type Hamiltonian, which considers the excitons as “system” and the vibrational states of the molecule as environment (“bath”) (May and Kühn 2008). For LHCs the excitonic couplings, temperature, and reorganization energy can be of comparable magnitude, which precludes the application of weak coupling approximations. The hierarchical equation of motion (HEOM) method introduced by Tanimura and Kubo (1989) solves the Frenkel exciton-model dynamics in an exact way and does not rely on small parameter assumption (Ishizaki and Fleming 2009; Kreisbeck et al. 2011). A comprehensive comparison of Redfield and HEOM spectra for the Fenna-Matthews-Olson (FMO) complex is given by Hein et al. (2012); Kramer et al. (2018b), for the Photosystem I supercomplex and Foerster theory by Kramer et al. (2018a), and for combined Foerster-Redfield theory applied to the light har-

Tobias Kramer
Zuse Institute Berlin, Germany E-mail: kramer@zib.de (corresponding author)

Mirta Rodríguez
Zuse Institute Berlin, Germany E-mail: rodriguez@zib.de

(k, l, m, n)	$C_{klmn} \langle 0^\circ, 0^\circ, 0^\circ, 0^\circ \rangle$
(1, 1, 2, 2), (1, 1, 3, 3), (1, 2, 1, 2), (1, 2, 2, 1), (1, 3, 1, 3), (1, 3, 3, 1)	$+\frac{1}{15}$
(2, 1, 1, 2), (2, 1, 2, 1), (2, 2, 1, 1), (2, 2, 3, 3), (2, 3, 2, 3), (2, 3, 3, 2)	$+\frac{1}{15}$
(3, 1, 1, 3), (3, 1, 3, 1), (3, 2, 2, 3), (3, 2, 3, 2), (3, 3, 1, 1), (3, 3, 2, 2)	$+\frac{1}{15}$
(1, 1, 1, 1), (2, 2, 2, 2), (3, 3, 3, 3)	$+\frac{1}{5}$
(k, l, m, n)	$C_{klmn} \langle 45^\circ, -45^\circ, 90^\circ, 0^\circ \rangle$
(1, 2, 1, 2), (1, 2, 2, 1), (1, 3, 1, 3)	$+\frac{1}{12}, -\frac{1}{12}, +\frac{1}{12}$
(1, 3, 3, 1), (2, 1, 1, 2), (2, 1, 2, 1)	$-\frac{1}{12}, -\frac{1}{12}, +\frac{1}{12}$
(2, 3, 2, 3), (2, 3, 3, 2), (3, 1, 1, 3)	$+\frac{1}{12}, -\frac{1}{12}, -\frac{1}{12}$
(3, 1, 3, 1), (3, 2, 2, 3), (3, 2, 3, 2)	$+\frac{1}{12}, -\frac{1}{12}, +\frac{1}{12}$

Table 1 C_{klmn} coefficients for isotropic averaging of the $\langle 0^\circ, 0^\circ, 0^\circ, 0^\circ \rangle$ and $\langle 45^\circ, -45^\circ, 90^\circ, 0^\circ \rangle$ polarization sequences

vesting complex II (LHCII) by Kreisbeck et al. (2014); Novoderezhkin and van Grondelle (2017).

Here, we discuss how the protein structures of LHCs are reflected in 2DES for different pulse polarizations and how rotational and static disorder affects the spectra. This analysis is required to interpret sequences of 2DES in terms of signature of coherent exciton dynamics.

2 Two-dimensional electronic spectra (2DES)

Most commonly 2DES is applied in the “all parallel” setup, where all pulses are polarized along the same direction. In this case, 2DES provides direct insights in to the dynamics of the excitonic energy transfer, since the stimulated emission (SE) and excited state absorption (ESA) signals trace the population dynamics of exciton states during the delay time T_2 between the second and third pulse. For the FMO complex contained in green sulfur bacteria (Olson and a Romano 1962; Fenna and Matthews 1975; Blankenship 2014), the transfer dynamics mirrored in 2DES has been analyzed with HEOM by Chen et al. (2011); Hein et al. (2012); Kreisbeck and Kramer (2012). In contrast to the SE/ESA contributions, the ground state bleaching (GSB) pathway mirrors the linear absorption signal at long delay times and does not provide direct insights into the population dynamics (Kramer and Rodríguez 2017). However, GSB is particularly susceptible to vibrational motion, which enters the 2DES (Tiwari et al. 2013; Kreisbeck et al. 2013) and produces beating signals in the cross-peak amplitudes as function of the delay time T_2 . These oscillatory signals have been observed by Engel et al. (2007) in experimental 2DES and need to be separated from electronic coherences. Over the years various polarization sequences have been explored to disentangle the overlapping and oscillating peaks composing a typical 2DES.

2.1 Polarization sequences

The 2DES of light harvesting complexes often shows large and overlapping regions, making it difficult to directly assign peaks to single excitonic energies. Various extension of 2DES have been proposed, see the reviews by (Nuernberger et al. 2015; Lambrev et al. 2019) and have been used to isolate specific features in the spectra. To confirm the structural information of LHCs obtained from crystals (Tronrud et al. 2009) and electron microscopy (Bína et al. 2016), circular and linear dichroism studies are important to probe the relative orientations of the transition dipole moments (Lindorfer and Renger 2018). By choosing specific polarization sequences, 2DES is also suitable to interrogate the molecular configuration (orientation and magnitude) of the transition-dipole moments. To see this, we consider exemplary the stimulated emission rephasing (SE,RP) pathway (see Kramer et al. (2018b), Eq. (65)):

$$S_{\text{SE,RP}}(T_3, T_2, T_1 | p_0, p_1, p_2, p_3) = \text{iTr}[\hat{\mu}_{p_3}^-(t_3)\hat{\mu}_{p_1}^+(t_1)\rho_0\hat{\mu}_{p_0}^-(0)\hat{\mu}_{p_2}^+(t_2)], \quad (1)$$

with time intervals $T_1 = t_1$, $T_2 = t_2 - t_1$, $T_3 = t_3 - t_2$ and four impulsive interactions of the excitonic states with the light pulses represented by the dipole operators μ with polarizations p_i . The recorded electric field of the signal is given by the sum of all pathways and incurs an additional conjugation (see Hamm and Zanni (2011), Eq. (4.29)):

$$E_{\text{sig}} \propto \text{i} (S_{\text{GSB,RP}} + S_{\text{SE,RP}} + S_{\text{ESA,RP}}). \quad (2)$$

Within the HEOM method the time-propagation of the coupled exciton-vibrational system is performed numerically. The first T_1 and last T_3 interval of the time-dependent signal (1) are Fourier transformed to the frequency domain and represents the excitation (ω_1) and emission (ω_3) frequencies. To account for an ensemble of randomly oriented molecules, a rotational isotropic average of the signal has to be performed. This leads to a tensorial expression of all possible directional Cartesian

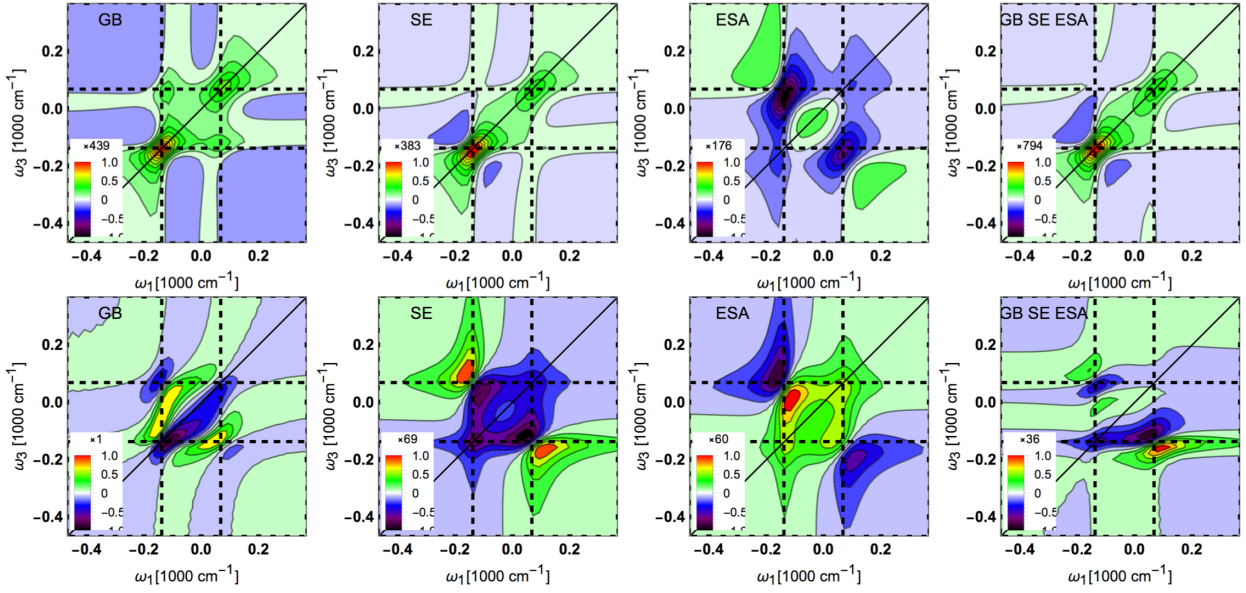


Fig. 1 Calculated 2DES of a dimer. Upper row: Real part of the rephasing signal for $\langle 0^\circ, 0^\circ, 0^\circ, 0^\circ \rangle$ polarization sequence at delay time $T_2 = 40$ fs, lower row, same for the $\langle 45^\circ, -45^\circ, 90^\circ, 0^\circ \rangle$ polarizations. From left to right the contributions of the different pathways are shown, the value above the color bar indicates the magnitude of the signal. The right panels show the combined, experimentally accessible signal. In the all-parallel sequence diagonal peaks are enhanced, while in the $\langle 45^\circ, -45^\circ, 90^\circ, 0^\circ \rangle$ sequence the cross-peaks are visible with additional zero crossings.

components, which is however reduced by symmetry to 21 terms at most (Gordon 1968; Yuen-Zhou et al. 2014; Gelin et al. 2017; Kramer et al. 2018b). Upon transforming the time trace to the frequency domain and isotropic rotational average we obtain

$$\begin{aligned} \langle S_{\text{RP}}(\omega_3, T_2, \omega_1) \rangle_{\text{rot}} &= \int_0^\infty dT_1 \int_0^\infty dT_3 e^{-iT_1 \omega_1 + iT_3 \omega_3} \\ &\times \sum_{k,l,m,n=1}^3 C_{klmn} S_{\text{SE,RP}}(T_3, T_2, T_1 | p_{0,k}, p_{1,l}, p_{2,m}, p_{3,n}). \end{aligned} \quad (3)$$

The C_{klmn} coefficients are determined by

$$\begin{aligned} C_{klmn} &= \\ &\delta_{kl} \delta_{mn} [(\mathbf{f}_0 \mathbf{f}_1)(\mathbf{f}_2 \mathbf{f}_3) - (\mathbf{f}_0 \mathbf{f}_2)(\mathbf{f}_1 \mathbf{f}_3) - (\mathbf{f}_0 \mathbf{f}_3)(\mathbf{f}_1 \mathbf{f}_2)] / 30 \\ &+ \delta_{km} \delta_{ln} [(\mathbf{f}_0 \mathbf{f}_2)(\mathbf{f}_1 \mathbf{f}_3) - (\mathbf{f}_0 \mathbf{f}_1)(\mathbf{f}_2 \mathbf{f}_3) - (\mathbf{f}_0 \mathbf{f}_3)(\mathbf{f}_1 \mathbf{f}_2)] / 30 \\ &+ \delta_{kn} \delta_{lm} [(\mathbf{f}_0 \mathbf{f}_3)(\mathbf{f}_1 \mathbf{f}_2) - (\mathbf{f}_0 \mathbf{f}_1)(\mathbf{f}_2 \mathbf{f}_3) - (\mathbf{f}_0 \mathbf{f}_2)(\mathbf{f}_1 \mathbf{f}_3)] / 30, \end{aligned}$$

where \mathbf{f}_i denotes the unit vector of the electric field of the i th pulse. The rotational average can be used to address specific dipole combinations. To simulate the experimental ensemble requires additionally to account for slower conformational variations of the chromophores (for instance bending and twisting modes), which lead to fluctuations of the site energies, known as static disorder. Static disorder requires to run simulations for different site energies and leads to a further

blurring of the 2DES, albeit with different effects at changing locations in the ω_1 - ω_3 frequency-plane.

The $\langle 0^\circ, 0^\circ, 0^\circ, 0^\circ \rangle$ polarization sequence

In the all parallel polarization sequence, GSB and the combined SE+ESA pathways contribute with similar magnitude to the total 2DES signal, see the analysis of the 2DES of *C. tepidum* by Kramer and Rodriguez (2017), Fig. 3. The isotropic averaging coefficients are listed in Tab. 1. Typical 2DES of FMO for the $\langle 0^\circ, 0^\circ, 0^\circ, 0^\circ \rangle$ polarization sequence computed with DM-HEOM (Noack et al. 2018; Kramer et al. 2018b) are shown in Kramer et al. (2018b), Fig. 11. The Hamiltonian and the dipole directions are listed in Kramer et al. (2018b), Tab. 1 and Eq. (77), taken from Adolphs and Renger (2006). The energy transfer is clearly visible in experiments performed by Brixner et al. (2005) and in theoretical computations (Hein et al. 2012; Kreisbeck and Kramer 2012) in form of the growing intensities of the lower cross peaks compared to the diagonal peaks. On top of the energy decay Engel et al. (2007); Panitchayangkoon et al. (2010) reported oscillatory amplitudes, which are interpreted as a combination of ground-state bleach induced vibrational modes and electronic coherences. The electronic coherences are expected to decay on the time-scale of the combined dephasing and relaxation decoherence time (Kreisbeck

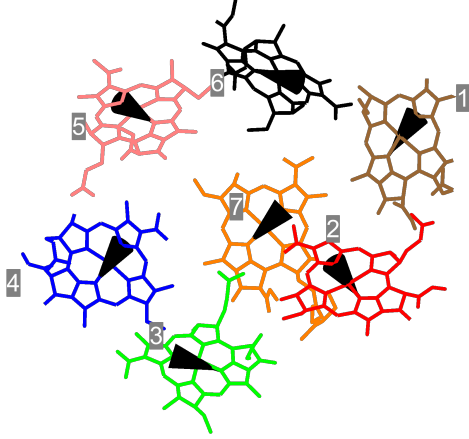


Fig. 2 The orientations of the transition dipoles in the Fenna-Matthews-Olson complex (FMO monomeric unit 3ENI) along the N_B and N_D nitrogens.

and Kramer 2012) of the two eigenenergies at the location of cross-peak. The slope of the spectral density towards zero frequency determines the pure dephasing time, while the value of the spectral density at the eigenenergies sets the relaxation rate. Both contribute to the decay time, see Kreisbeck and Kramer (2012), SI, and Kramer and Kreisbeck (2014), Fig. 8. Another manifestation of the spectral density $J(\omega)$ of each pigment m in 2DES is the reorganization energy λ_m :

$$\lambda_m = \int_0^\infty \frac{J_m(\omega)}{\pi\omega} d\omega. \quad (4)$$

The reorganization energy leads to a downward shift of the diagonal and cross peaks with increasing delay (Dostál et al. 2016; Kramer and Rodríguez 2017). The observed shift is consistent with the organization energies around 40/cm assigned by (Adolphs and Renger 2006) to the bacteriochlorophylls contained in the FMO complex.

The $\langle 45^\circ, -45^\circ, 90^\circ, 0^\circ \rangle$ polarization sequence

Different polarization directions have been used by Hochstrasser (2001); Zanni et al. (2001) to enhance various features in 2D IR spectra and 2DES (Schlau-Cohen et al. 2012). For a polarization sequence with two orthogonal pulse pairs, the isotropic rotational averaging suppresses the (1, 1, 1, 1), (2, 2, 2, 2), and (3, 3, 3, 3) components, and leads to alternating signs of the remaining 12 contributions listed in in Tab. 1 for the $\langle 45^\circ, -45^\circ, 90^\circ, 0^\circ \rangle$ case. This selection of pathways eliminates the ground-state bleaching signal (Westenhoff et al. 2012) and emphasizes all dipole pairs with orthogonal orientation. To demonstrate this, we derive an

approximate expression for the 2DES of a dimer with dipole directions given by \mathbf{D}_1 , \mathbf{D}_2 and Hamiltonian

$$H_{\text{dimer}} = \begin{pmatrix} -E & J \\ J & +E \end{pmatrix} \quad (5)$$

with eigenvalues $\{-\Delta E/2, +\Delta E/2 = \sqrt{E^2 + J^2}\}$. An analytic expression for the 2DES is obtained by considering a purely coherent dynamics for the density matrix

$$\rho(t) = e^{-iH(t-t_0)/\hbar} \rho(t_0) e^{+iH(t-t_0)/\hbar}, \quad (6)$$

and only introducing decoherence through the inverse of the decoherence time $\alpha = 1/\tau_{\text{decoherence}}$. Inserting the time-evolution in Eq. (6) yields the time-representation of the rephasing signal

$$\text{SERP}_{4490}(T_1, T_2, T_3) = 2(\mathbf{D}_1 \times \mathbf{D}_2)^2 \cos\left(\sqrt{E^2 + J^2}(T_1 + 2T_2 + T_3)\right) e^{-\alpha(T_1 + T_2 + T_3)}. \quad (7)$$

The cross product of the two transition-dipole directions in Eq. (7) leads to a vanishing contribution of any parallel dipole component. The Fourier transform to the frequency domain results in

$$\begin{aligned} \text{SERP}_{4490}(\omega_1, T_2, \omega_3) &= (\mathbf{D}_1 \times \mathbf{D}_2)^2 \\ &\times \left[\frac{(2\omega_1 - \Delta E^+)(\Delta E^+ + 2\omega_3)e^{-i\Delta E T_2}}{\Gamma} \right. \\ &\quad \left. - \frac{(\Delta E^+ + 2\omega_1)(\Delta E^+ - 2\omega_3)e^{i\Delta E T_2}}{\Gamma} \right], \\ \Gamma &= 2\pi(\Delta E^- - 2\omega_3)(-\Delta E^+ - 2\omega_3) \\ &\quad \times (J^2 - (E^- + \omega_1)(\omega_1 - E^+)), \end{aligned} \quad (8)$$

where we introduced $\Delta E^\pm = \Delta E \pm i2\alpha$, $E^\pm = E \pm i\alpha$. At the cross peak location this expression simplifies to

$$\begin{aligned} \text{SERP}_{4490}(\omega_1 = \Delta E/2, T_2, \omega_3 = -\Delta E/2) &= \\ &- \frac{(\mathbf{D}_1 \times \mathbf{D}_2)^2}{2\pi\alpha^2} \left(e^{-iT_2\Delta E/\hbar} - \frac{\alpha^2 e^{iT_2\Delta E/\hbar}}{(\Delta E + i\alpha)^2} \right). \end{aligned} \quad (9)$$

The ESA rephasing term has the same form (up to an overall sign), albeit with a slightly different decoherence parameter α' due to the coupling to the vibrational states of two separated pigments. The observed signal is the real part of the difference of the SE and ESA pathways and brings along an additional sign change in the ω_1, ω_3 plane, see Fig. 1 for a model dimer with energies $E = 50 \text{ cm}^{-1}$ and couplings $J = -90 \text{ cm}^{-1}$. This results in alternating stripes of positive/negative contributions and shifts the highest/lowest intensities away from the cross-peak locations already in the individual pathways (SE, ESA). This is in contrast to the all-parallel polarization sequence, where ESA has only negative components and SE positive values, which largely stay in place.

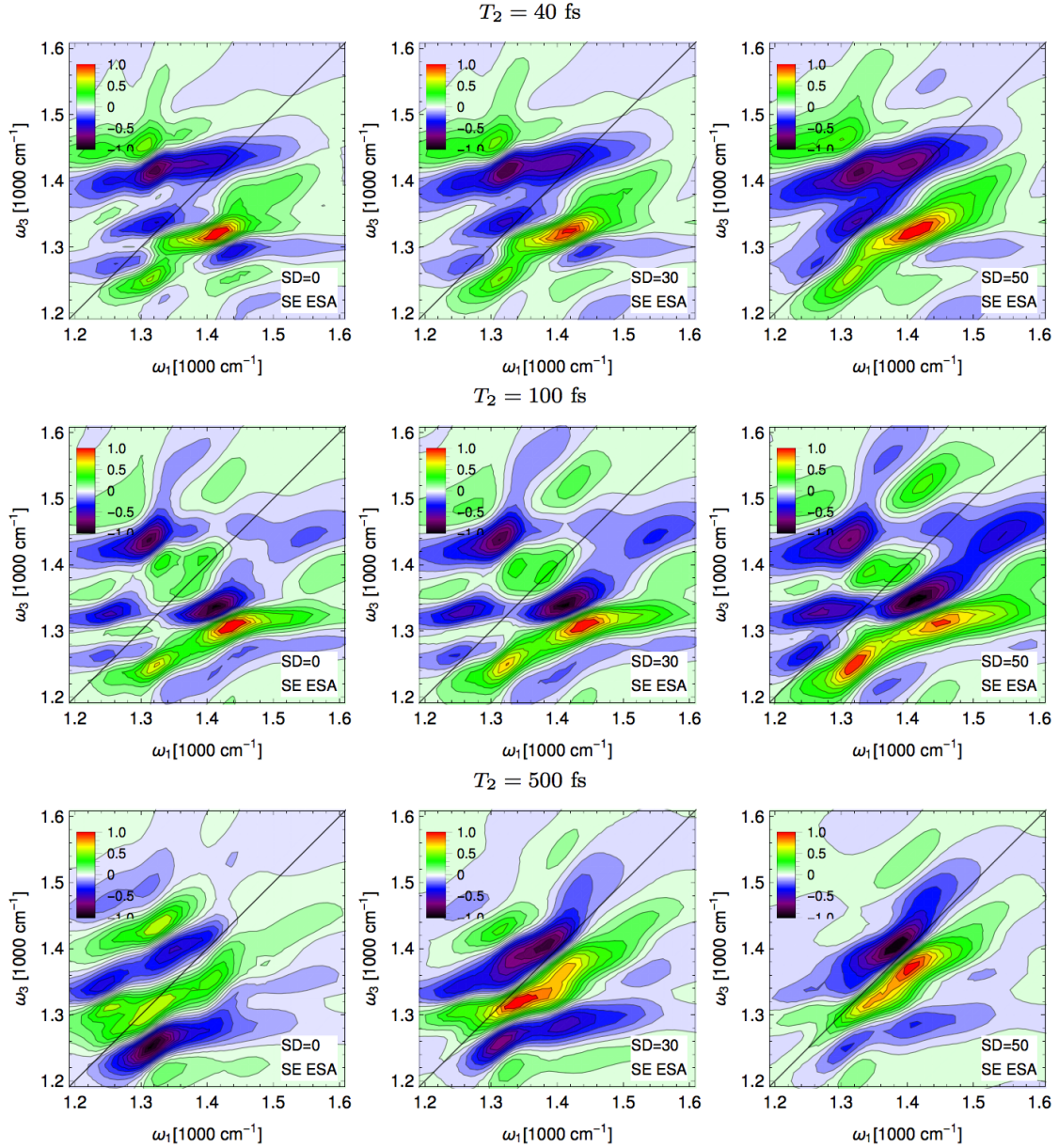


Fig. 3 Calculated 2DES of FMO for delay times $T_2 = \{40, 100, 500\}$ fs. Imaginary part of the rephasing signal for $\langle 45^\circ, -45^\circ, 90^\circ, 0^\circ \rangle$ polarization sequence for increasing values of static disorder (SD), $\{0, 30, 50\}$ cm^{-1} , temperature $T = 100$ K. See Fig. 5 by Rodríguez and Kramer (2019) for the real part of the rephasing signal. Corresponding measured spectra by Thyryhaug et al. (2018) are shown in their Fig. 2c, SI Fig. 2a, SI Fig. 2b and favor the 30 – 50 cm^{-1} static disorder cases. This results in alternating stripes aligned along the diagonal.

The selective excitation of orthogonal dipole orientations leads to a different 2DES of the FMO complex compared to the all-parallel polarization sequence. In the FMO complex, the transition dipoles are aligned within a few degrees with the nitrogen atoms N_B - N_D in the bacteriochlorophylls, see Fig. 2. The dipoles of bacteriochlorophyll pairs (1, 3), (1, 5), (2, 7), (3, 4), (4, 5), (5, 7) are almost orthogonally arranged, but strong excitonic couplings in conjunction to the orthogonal direc-

tions are only existing between the neighbouring pigments (3, 4), (4, 5) (Vulto et al. 1998, 1999; Adolphs et al. 2008). The $\langle 45^\circ, -45^\circ, 90^\circ, 0^\circ \rangle$ sequence thus enhances the contribution of these specific pairs of bacteriochlorophylls in the complex, however at the added complexity of alternating signs in the signal, which are strongly affected by static disorder. Thyryhaug et al. (2016) measured 2DES with another polarization sequence, taken to be $\langle 90^\circ, 90^\circ, 0^\circ, 0^\circ \rangle$. Corresponding com-

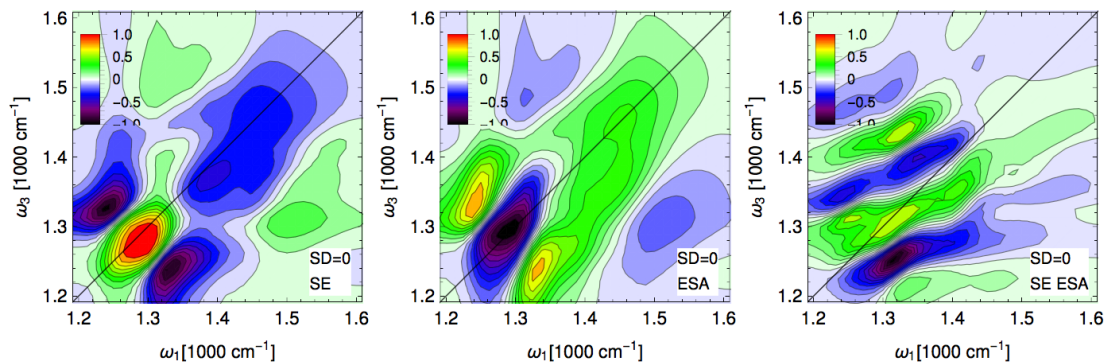


Fig. 4 Calculated 2DES of FMO. Imaginary part of the rephasing signal for the $\langle 45^\circ, -45^\circ, 90^\circ, 0^\circ \rangle$ polarization sequence at 500 fs delay time in the absence of static disorder. Shown is the decomposition of the experimentally accessible signal (sum of SE and ESA, resulting in stripes) into the SE and ESA components (GSB does not contribute).

puted 2DES are discussed by Kramer et al. (2018b), Fig. 12.

While the $\langle 45^\circ, -45^\circ, 90^\circ, 0^\circ \rangle$ sequence has been suggested and used for studying cross-peak dynamics in FMO, it is more prone to disorder average than the all-parallel configuration. The alternating signs of the stripes in the real part of the rephasing signal of the $\langle 45^\circ, -45^\circ, 90^\circ, 0^\circ \rangle$ sequence tend to diminish the signal and only elongated stripes along the diagonal remain. Numerically, we compute the disorder average from 5000 realizations of disorder added to the site energies with standard deviation 30 cm^{-1} and 50 cm^{-1} . The resulting 2DES are efficiently encoded in a neural network representation following Rodríguez and Kramer (2019). This encoding allows us to study various disorder realizations, shown in Fig. 3 for delay times $T_2 = 40 \text{ fs}$, 100 fs , and 500 fs .

The total 2DES is the addition of SE and ESA contributions (see Fig. 4) and develops a stripe-like pattern. Note, that in the experimental signals recorded by Thyryhaug et al. (2018) Supplementary Fig. 2 (corresponding to the lower two panels in Fig. 3) the stripes are almost perfectly parallel to the diagonal, already at shorter delay times (100 fs) compared to the simulation. A similar theoretical spectrum for the 40 fs delay time is shown by Thyryhaug et al. (2018), Fig. 2d, computed with a stochastic averaging approach instead of the tensorial method used here.

3 Conclusion

The understanding of 2DES of LHCs requires to ensemble average individual molecular complexes over rotational and static disorder. This averaging process has been used experimentally in combination with specific polarization sequences with the goal to enhance cer-

tain relative pigment orientations (see Thyryhaug et al. (2016, 2018)). Our calculations of FMO spectra show that the cross-peaks in these sequences are diminished and split by cancellation effects of positive/negative signal contributions from the SE and ESA pathways. With increasing static disorder elongated structures arise and blur specific cross-peak contributions. The disorder sensitivity is different compared to the all-parallel 2DES polarization which causes less cancellations due to sign changes in the signal, but is directly affected by broadening of peaks due to static disorder.

The 2DES of the FMO complex demonstrate that the theoretical models of the exciton energy transfer are in general agreement with the experimental observations. This includes the values for the excitonic couplings, site energies, and vibrational density of states. The excitonic, vibrational and reorganization energies derived from theory and experiment bring along electronic coherences, typically decaying within 300 fs at ambient temperatures (Kreisbeck and Kramer 2012). The functional role of these coherences is still debated since Avery et al. (1961). Kramer and Kreisbeck (2014) find that resonances between vibrational states and electronic energy differences can either hinder or enhance transfer times.

For LHCs with more pigments a simultaneous fitting of 2DES, circular and linear dichroism, and transient absorption spectra will be required to further interpret the experimental data and to provide systematic predictions. A recent review by Lambrev et al. (2019) of the experimental and theoretical 2DES of LHCs comes to a similar conclusion, especially for the light harvesting complex II (LHC II).

Conflict of Interest: The authors declare that they have no conflict of interest.

Acknowledgements The work was supported by the German Research Foundation (DFG) grants KR 2889 and RE 1389 (“Realistic Simulations of Photoactive Systems on HPC Clusters with Many-Core Processors”). We acknowledge compute time allocation by the North-German Supercomputing Alliance (HLRN). M.R. has received funding from the European Union’s Horizon 2020 research and innovation programme under the Marie Skłodowska-Curie grant agreement No. 707636.

References

- Adolphs J, Renger T (2006) How Proteins Trigger Excitation Energy Transfer in the FMO Complex of Green Sulfur Bacteria. *Biophysical Journal* 91(8):2778–2797, DOI 10.1529/biophysj.105.079483
- Adolphs J, Müh F, Madjet MEA, Renger T (2008) Calculation of pigment transition energies in the FMO protein. *Photosynthesis Research* 95(2-3):197–209, DOI 10.1007/s11120-007-9248-z
- Aghtar M, Strümpfer J, Olbrich C, Schulten K, Kleinekathöfer U (2013) The FMO Complex in a Glycerol–Water Mixture. *The Journal of Physical Chemistry B* 117(24):7157–7163, DOI 10.1021/jp311380k
- Avery J, Bay Z, Szent-Gyorgyi A (1961) On the Energy Transfer in Biological Systems. *Proceedings of the National Academy of Sciences of the United States of America* 47(11):1742–1744
- Bína D, Gardian Z, Vácha F, Litvín R (2016) Native FMO-reaction center supercomplex in green sulfur bacteria: An electron microscopy study. *Photosynthesis Research* 128(1):93–102, DOI 10.1007/s11120-015-0205-y
- Blankenship RE (2014) *Molecular Mechanisms of Photosynthesis*, 2nd edn. Wiley, Oxford, UK
- Brixner T, Stenger J, Vaswani HM, Cho M, Blankenship RE, Fleming GR (2005) Two-dimensional spectroscopy of electronic couplings in photosynthesis. *Nature* 434(7033):625–628, DOI 10.1038/nature03429
- Chen L, Zheng R, Jing Y, Shi Q (2011) Simulation of the two-dimensional electronic spectra of the Fenna-Matthews-Olson complex using the hierarchical equations of motion method. *The Journal of Chemical Physics* 134(19):194508–194508, DOI 10.1063/1.3589982
- Cho M (2008) Coherent Two-Dimensional Optical Spectroscopy. *Chemical Reviews* 108(4):1331–1418, DOI 10.1021/cr078377b
- Dostál J, Pšenčík J, Zigmantas D (2016) In situ mapping of the energy flow through the entire photosynthetic apparatus. *Nature Chemistry* 8(7):705–710, DOI 10.1038/nchem.2525
- Engel GS, Calhoun TR, Read EL, Ahn TK, Mančal T, Cheng YC, Blankenship RE, Fleming GR (2007) Evidence for wavelike energy transfer through quantum coherence in photosynthetic systems. *Nature* 446(7137):782–786, DOI 10.1038/nature05678
- Fenna RE, Matthews BW (1975) Chlorophyll arrangement in a bacteriochlorophyll protein from *Chlorobium limicola*. *Nature* 258(5536):573–577, DOI 10.1038/258573a0
- Gelin MF, Borrelli R, Domcke W (2017) Efficient orientational averaging of nonlinear optical signals in multichromophore systems. *The Journal of Chemical Physics* 147(4):044114–044114, DOI 10.1063/1.4996205
- Gordon R (1968) Correlation Functions for Molecular Motion. In: *Advances in Magnetic and Optical Resonance*, vol 3, ACADEMIC PRESS INC., pp 1–42, DOI 10.1016/B978-1-4832-3116-7.50008-4
- Hamm P, Zanni MT (2011) *Concepts of 2D Spectroscopy*. Cambridge University Press, Cambridge
- Hein B, Kreisbeck C, Kramer T, Rodríguez M (2012) Modelling of oscillations in two-dimensional echo-spectra of the Fenna-Matthews-Olson complex. *New Journal of Physics* 14(2):023018–023018, DOI 10.1088/1367-2630/14/2/023018
- Hochstrasser RM (2001) Two-dimensional IR-spectroscopy: Polarization anisotropy effects. *Chemical Physics* 266(2-3):273–284, DOI 10.1016/S0301-0104(01)00232-4
- Ishizaki A, Fleming GR (2009) On the adequacy of the Redfield equation and related approaches to the study of quantum dynamics in electronic energy transfer. *The Journal of Chemical Physics* 130(23):234110–234110, DOI 10.1063/1.3155214
- Kramer T, Kreisbeck C (2014) Modelling excitonic-energy transfer in light-harvesting complexes. *AIP Conference Proceedings* 1575:111–135, DOI 10.1063/1.4861701
- Kramer T, Rodríguez M (2017) Two-dimensional electronic spectra of the photosynthetic apparatus of green sulfur bacteria. *Scientific Reports* 7:45245–45245, DOI 10.1038/srep45245
- Kramer T, Noack M, Reimers JR, Reinefeld A, Rodríguez M, Yin S (2018a) Energy flow in the Photosystem I supercomplex: Comparison of approximative theories with DM-HEOM. *Chemical Physics* 515:262–271, DOI 10.1016/j.chemphys.2018.05.028
- Kramer T, Noack M, Reinefeld A, Rodríguez M, Zelinskyy Y (2018b) Efficient calculation of open quantum system dynamics and time-resolved spectroscopy with distributed memory HEOM (DM-HEOM). *Journal of Computational Chemistry* 39(22):1779, DOI 10.1002/jcc.25354
- Kreisbeck C, Kramer T (2012) Long-lived electronic coherence in dissipative exciton dynamics of light-harvesting complexes. *Journal of Physical Chemistry Letters* 3(19):2828–2833, DOI 10.1021/jz3012029
- Kreisbeck C, Kramer T, Rodríguez M, Hein B (2011) High-performance solution of hierarchical equations of motion for studying energy transfer in light-harvesting complexes. *Journal of Chemical Theory and Computation* 7(7):2166–2174, DOI 10.1021/ct200126d
- Kreisbeck C, Kramer T, Aspuru-Guzik A (2013) Disentangling electronic and vibronic coherences in two-dimensional echo spectra. *Journal of Physical Chemistry B* 117(32):9380–9385, DOI 10.1021/jp405421d
- Kreisbeck C, Kramer T, Aspuru-Guzik A (2014) Scalable High-Performance Algorithm for the Simulation of Exciton Dynamics. Application to the Light-Harvesting Complex II in the Presence of Resonant Vibrational Modes. *Journal of Chemical Theory and Computation* 10:4045–4054, DOI 10.1021/ct500629s
- Lambrev PH, Akhtar P, Tan HS (2019) Insights into the mechanisms and dynamics of energy transfer in plant light-harvesting complexes from two-dimensional electronic spectroscopy. *Biochimica et Biophysica Acta (BBA) - Bioenergetics* DOI 10.1016/j.bbabo.2019.07.005
- Lindorfer D, Renger T (2018) Theory of Anisotropic Circular Dichroism of Excitonically Coupled Systems: Application to the Baseplate of Green Sulfur Bacteria. *The Journal of Physical Chemistry B* 122(10):2747–2756, DOI 10.1021/acs.jpcc.7b12832
- May V, Kühn O (2008) Optical field control of charge transmission through a molecular wire. I. Generalized master equation description. *Physical Review B* 77(11):115439–115439, DOI 10.1103/PhysRevB.77.115439

- Mukamel S (1995) *Principles of Nonlinear Optical Spectroscopy*. Oxford University Press, Oxford
- Noack M, Reinefeld A, Kramer T, Steinke T (2018) DM-HEOM: A Portable and Scalable Solver-Framework for the Hierarchical Equations of Motion. 2018 IEEE International Parallel and Distributed Processing Symposium Workshops (IPDPSW) p 947, DOI 10.1109/IPDPSW.2018.00149
- Novoderezhkin VI, van Grondelle R (2017) Modeling of excitation dynamics in photosynthetic light-harvesting complexes: Exact versus perturbative approaches. *Journal of Physics B: Atomic, Molecular and Optical Physics* 50(12):124003–124003, DOI 10.1088/1361-6455/aa6b87
- Nuernberger P, Ruetzel S, Brixner T (2015) Multidimensional Electronic Spectroscopy of Photochemical Reactions. *Angewandte Chemie International Edition* 54(39):11368–11386, DOI 10.1002/anie.201502974
- Olbrich C, Jansen TLC, Liebers J, Aghtar M, Strümpfer J, Schulten K, Knoester J, Kleinekathöfer U (2011) From atomistic modeling to excitation transfer and two-dimensional spectra of the FMO light-harvesting complex. *Journal of Physical Chemistry B* 115(26):8609–8621, DOI 10.1021/jp202619a
- Olson JM, a Romano C (1962) A new chlorophyll from green bacteria. *Biochimica et Biophysica Acta* 59(3):726–728, DOI 10.1016/0006-3002(62)90659-5
- Panitchayangkoon G, Hayes D, a Fransted K, Caram JR, Harel E, Wen J, Blankenship RE, Engel GS (2010) Long-lived quantum coherence in photosynthetic complexes at physiological temperature. *Proceedings of the National Academy of Sciences of the United States of America* 107(29):12766–70, DOI 10.1073/pnas.1005484107
- Rodríguez M, Kramer T (2019) Machine learning of two-dimensional spectroscopic data. *Chemical Physics* 520:52–60, DOI 10.1016/j.chemphys.2019.01.002
- Schlau-Cohen GS, Ishizaki A, Calhoun TR, Ginsberg NS, Ballottari M, Bassi R, Fleming GR (2012) Elucidation of the timescales and origins of quantum electronic coherence in LHCII. *Nature Chemistry* 4(5):389–395, DOI 10.1038/nchem.1303
- Tanimura Y, Kubo R (1989) Time Evolution of a Quantum System in Contact with a Nearly Gaussian-Markoffian Noise Bath. *Journal of the Physics Society Japan* 58(1):101–114, DOI 10.1143/JPSJ.58.101
- Thyrhaug E, Židek K, Dostál J, Bína D, Zigmantas D (2016) Exciton Structure and Energy Transfer in the Fenna–Matthews–Olson Complex. *The Journal of Physical Chemistry Letters* 7(9):1653–1660, DOI 10.1021/acs.jpclett.6b00534
- Thyrhaug E, Tempelaar R, Alcocer MJP, Židek K, Bína D, Knoester J, Jansen TLC, Zigmantas D (2018) Identification and characterization of diverse coherences in the Fenna–Matthews–Olson complex. *Nature Chemistry* 10(7):780–786, DOI 10.1038/s41557-018-0060-5
- Tiwari V, Peters WK, Jonas DM (2013) Electronic resonance with anticorrelated pigment vibrations drives photosynthetic energy transfer outside the adiabatic framework. *Proceedings of the National Academy of Sciences* 110(4):1203–1208, DOI 10.1073/pnas.1211157110
- Tronrud DE, Wen J, Gay L, Blankenship RE (2009) The structural basis for the difference in absorbance spectra for the FMO antenna protein from various green sulfur bacteria. *Photosynthesis Research* 100(2):79–87, DOI 10.1007/s11120-009-9430-6
- Vulto SIE, de Baat MA, Louwe RJW, Permentier HP, Neef T, Miller M, van Amerongen H, Aartsma TJ (1998) Exciton Simulations of Optical Spectra of the FMO Complex from the Green Sulfur Bacterium *Chlorobium tepidum* at 6 K. *The Journal of Physical Chemistry B* 102(47):9577–9582, DOI 10.1021/jp982095l
- Vulto SIE, de Baat MA, Neerken S, Nowak FR, van Amerongen H, Ames J, Aartsma TJ (1999) Excited State Dynamics in FMO Antenna Complexes from Photosynthetic Green Sulfur Bacteria: A Kinetic Model. *The Journal of Physical Chemistry B* 103(38):8153–8161, DOI 10.1021/jp984702a
- Westenhoff S, Palecek D, Edlund P, Smith P, Zigmantas D (2012) Coherent Picosecond Exciton Dynamics in a Photosynthetic Reaction Center. *Journal of the American Chemical Society* 134(40):16484–16487, DOI 10.1021/ja3065478
- Yuen-Zhou J, Krich JJ, Kassal I, Johnson A, Aspuru-Guzik A (2014) Ultrafast Spectroscopy. IOP Publishing, DOI 10.1088/978-0-750-31062-8
- Zanni MT, Ge NH, Kim YS, Hochstrasser RM (2001) Two-dimensional IR spectroscopy can be designed to eliminate the diagonal peaks and expose only the crosspeaks needed for structure determination. *Proceedings of the National Academy of Sciences* 98(20):11265–11270, DOI 10.1073/pnas.201412998